European Journal of Nuclear Medicine and Molecular Imaging
https://doi.org/10.1007/s00259-019-04569-0

ORIGINAL ARTICLE

^{18}F-PSMA-1007 multiparametric, dynamic PET/CT in biochemical relapse and progression of prostate cancer

Christos Sachpekidis[1,2] · A. Afshar-Oromieh[2,3] · K. Kopka[4,5] · D. S. Strauss[1] · L. Pan[1] · U. Haberkorn[1,3] · A. Dimitrakopoulou-Strauss[1]

Received: 8 July 2019 / Accepted: 3 October 2019

Abstract

Objectives Aim of the present analysis is to investigate the biodistribution and pharmacokinetics of the recently clinically introduced radioligand ^{18}F-PSMA-1007 in patients with biochemical recurrence or progression of prostate cancer (PC) by means of multiparametric (dynamic and whole-body) PET/CT.

Methods Twenty-five (25) patients with PC biochemical relapse or progression (median age = 66.0 years) were enrolled in the analysis. The median PSA value was 1.2 ng/mL (range = 0.1–237.3 ng/mL) and the median Gleason score was 7 (range = 6–10). All patients underwent dynamic PET/CT (dPET/CT) scanning (60 min) of the pelvis and lower abdomen as well as whole-body PET/CT with ^{18}F-PSMA-1007. PET/CT assessment was based on qualitative evaluation, SUV calculation, and quantitative analysis based on a two-tissue compartment model and fractal analysis.

Results 15/25 patients were PET-positive. Plasma PSA values in the ^{18}F-PSMA-1007 positive group were higher (median = 3.6 ng/mL; range = 0.2–237.3 ng/mL) than in the ^{18}F-PSMA-1007 negative group (median value = 0.7 ng/mL; range = 0.1–3.0 ng/mL). Semi-quantitative analysis in the PC lesions demonstrated a mean $SUV_{average}$ = 25.1 (median = 15.4; range = 3.5–119.2) and a mean SUV_{max} = 41.5 (median = 25.7; range = 3.8–213.2). Time–activity curves derived from dPET/CT revealed an increasing tracer accumulation during the 60 min of dynamic PET acquisition into the PC lesions, higher than in the urinary bladder and the colon. Significant correlations were observed between ^{18}F-PSMA-1007 uptake (SUV), influx, and fractal dimension (FD).

Conclusions ^{18}F-PSMA-1007 PET/CT could detect PC lesions in 60% of the patients of a mixed population, including also patients with very low PSA values. Higher PSA values were associated with a higher detection rate. Dynamic PET analysis revealed an increasing tracer uptake during the dynamic PET acquisition as well as high binding and internalization of the radiofluorinated PSMA ligand in the PC lesions.

Keywords ^{18}F-PSMA-1007 · Multiparametric · Dynamic PET/CT · Prostate cancer · Two-tissue compartment model

This article is part of the Topical Collection on Oncology – Genitourinary

✉ Christos Sachpekidis
christos_saxpe@yahoo.gr

[1] Clinical Cooperation Unit Nuclear Medicine, German Cancer Research Center (DKFZ), Im Neuenheimer Feld 280, D-69210 Heidelberg, Germany

[2] Department of Nuclear Medicine, Inselspital, Bern University Hospital, University of Bern, Bern, Switzerland

[3] Division of Nuclear Medicine, University of Heidelberg, Heidelberg, Germany

[4] Division of Radiopharmaceutical Chemistry, German Cancer Research Center (DKFZ), Heidelberg, Germany

[5] German Cancer Consortium (DKTK), Heidelberg, Germany

Introduction

Prostate-specific membrane antigen (PSMA)-targeted PET/CT represents a novel, highly promising imaging modality being applied increasingly in the current decade in prostate cancer (PC) management. In particular, PET/CT imaging with the ^{68}Ga-labeled tracer Glu-urea-Lys(Ahx)-HBED-CC (^{68}Ga-PSMA-11) has shown clinical value both in PC biochemical relapse and primary staging [1–7]. Nevertheless, non-invasive imaging with the ^{68}Ga-labeled PSMA radioligand faces some challenges: firstly, its limited production capacity via local gallium generators leads to restrictions in its availability. Secondly, the short physical half-life of ^{68}Ga (approximately 68 min) prevents a relatively massive production and

Published online: 14 November 2019

distribution of the radiotracer ^{68}Ga-PSMA-11, despite the nowadays available cyclotron-based production of ^{68}Ga [8]. Furthermore, the rapid tracer excretion from the urinary tract leads to a high ^{68}Ga-PSMA-11-associated accumulation of radioactivity in the bladder, which can hamper prostate evaluation and even mask the detection of PC local recurrence [9].

In this context, the development and introduction in clinical practice of the radiofluorinated PSMA ligands represents a logical approach to overcome these limitations associated with ^{68}Ga-PSMA-11. Moreover, the capability of central cyclotron production and the longer physical half-life of ^{18}F (approximately 110 min) can help overcome the major practical issues regarding ^{68}Ga production and distribution. The two most studied and recently clinically introduced ^{18}F-labeled PSMA ligands are the (2-(3-{1-carboxy-5-[(6-[^{18}F]fluoro-pyridine-3-carbonyl)-amino]-pentyl}-ureido)-pentanedioic acid) (^{18}F-DCFPyL) and (((3S,10S,14S)-1-(4-(((S)-4-carboxy-2-((S)-4-carboxy-2-(6-[^{18}F]fluoro-nicotinamido)butanamido)butanamido)methyl)phenyl)-3-(naphthalen-2-ylmethyl)-1,4,12-trioxo-2,5,11,13-tetraazahexadecane-10,14,16-tricarboxylic acid)) (^{18}F-PSMA-1007) [10]. In particular, ^{18}F-PSMA-1007 demonstrates the advantage of low background activity in the urinary bladder, rendering ^{18}F-PSMA-1007 PET/CT an attractive alternative to ^{68}Ga-labeled PSMA imaging[11]. The published data on ^{18}F-PSMA-1007 PET/CT examinations suggest an achievement of excellent image quality and a high potential for lesion localization both in newly diagnosed and biochemically recurrent PC patients [10, 12–15].

In the present retrospective study, we performed multiparametric PET/CT scanning with both dynamic and whole-body static acquisition with the radiotracer ^{18}F-PSMA-1007. Our aim was to evaluate the pharmacokinetics and distribution of ^{18}F-PSMA-1007 in a group of patients with biochemical recurrence or progression of PC.

Materials and methods

Patients

Twenty-five patients with a history of previously treated PC were studied with ^{18}F-PSMA-1007 for restaging purposes and were enrolled in this analysis. In particular, 17 patients showed biochemical recurrence after therapy with curative intent; these patients were not receiving any treatment at the time of scanning. The remaining eight patients showed biochemical progression of PC, demonstrated by a PSA increase; these patients were already under treatment (androgen deprivation therapy) at the time of the PET/CT scan. The median age of the studied cohort was 66 years (range = 48–84 years). The median PSA value was 1.2 ng/mL (range = 0.2–237.3 ng/mL), and the median primary Gleason score—available in 18 patients—was 7 (range = 6–10). Table 1 presents the analyzed characteristics of the patients investigated. The study was conducted in accordance with the declaration of Helsinki, and was approved by the Ethical Committee of the University of Heidelberg (S-253/2019). All patients gave written informed consent to undergo ^{18}F-PSMA-1007 PET/CT following the regulations of the German Pharmaceuticals Act §13(2b).

Multiparametric PET/CT–data acquisition

The patients were intravenously administered with a median of 237 MBq ^{18}F-PSMA-1007 injection solution (range = 131–266 MBq), which was radiosynthesized with the direct one-step radiolabeling approach as published previously [16].

A dedicated PET/CT system (Biograph mCT, 128 S, Siemens Co., Erlangen, Germany) with an axial field of view of 21.6 cm with TruePoint and TrueV, operated in a three-dimensional mode, was used. A multiparametric PET/CT was performed, which consisted of the dynamic part (dPET/CT studies) and the static part (whole body PET/CT studies). dPET/CT was performed over the pelvic area and the lower abdomen (field of view = 43.2 cm) for 60 min after i.v. injection of the radiotracer using a 24-frame protocol (10 frames of 30 s, 5 frames of 60 s, 5 frames of 120 s, and 4 frames of 600 s) and a multibed protocol (two bed positions). After the end of the dynamic PET acquisition, the patients were asked to urinate, and then additional whole-body static images (starting approximately at 70 min p.i.) from the skull to the feet were acquired with duration of 2 min per bed position for the emission scans. A low-dose attenuation CT (120 kV, 30 mA) was used for attenuation correction of the dynamic emission PET data and for image fusion. A second low-dose CT (120 kV, 30 mA) was performed after the end of the dynamic series covering the area from the skull to the feet in order to counteract patient movement after the dynamic series. Details about the scanning protocol have been described previously by our group [17].

Multiparametric data analysis: SUV evaluation, compartment and non-compartment analysis

Data analysis was based on qualitative (visual) analysis of the PET/CT scans, semi-quantitative evaluation based on SUV calculations, and quantitative analysis based on a two-tissue compartment model and fractal analysis.

Qualitative analysis was based on visual assessment of the ^{18}F-PSMA PET/CT scans. Two nuclear medicine physicians (CS, ADS) evaluated the areas with high ^{18}F-PSMA-1007 expression on transaxial, coronal, and sagittal images. Areas presenting with enhanced tracer uptake, apart from those in which an increased tracer uptake is considered physiological, were considered indicative for PC recurrence. Both readers were blinded for clinical data at the time of analysis.

Table 1 Characteristics of the patients investigated

Patient no.	Age (years)	PSA (ng/mL)	Gleason score	Local recurrence	Lymph node metastases	Bone metastases	Other metastases (lung, liver)	Previous treatment	Indication	Dosage (MBq)
1	71	0.18	10	1	1	1		Radical prostatectomy and radiotherapy	Relapse	252
2	75	0.62	7					Radical prostatectomy	Relapse	227
3	62	0.20	7					Radical prostatectomy	Relapse	249
4	69	1.87	Unknown	1				Radical prostatectomy, lymphadenectomy and radiotherapy	Relapse	252
5	77	0.48	7					Radical prostatectomy	Relapse	251
6	73	1.58	7		2			Radical prostatectomy and radiotherapy	Relapse	242
7	74	1.19	7		3		1 (lung)	Radical prostatectomy and radiotherapy	Relapse	223
8	65	0.97	Unknown					Radical prostatectomy and radiotherapy	Relapse	257
9	59	0.40	Unknown	1	1			Androgen deprivation therapy	Progression	229
10	65	7.00	10		>20			Chemotherapy (docetaxel), radiotherapy	Progression	223
11	79	7.28	9	1	>20			Radical prostatectomy, androgen deprivation therapy	Progression	241
12	72	0.76	7					Radical prostatectomy	Relapse	170
13	48	4.49	7	1				Hyperthermia, androgen deprivation therapy	Relapse	131
14	72	1.14	7		2	4		Radical prostatectomy and radiotherapy, Androgen deprivation therapy	Relapse	184
15	66	6.17	7		>20	>20	>20 (liver)	Radical prostatectomy, lymphadenectomy and radiotherapy, Androgen deprivation therapy	Progression	228
16	65	237.30	10		>20	>20		Radical prostatectomy and radiotherapy, Androgen deprivation therapy, Chemotherapy	Progression	237
17	63	0.75	7					Radical prostatectomy	Relapse	237
18	60	0.21	6					Radical prostatectomy	Relapse	266
19	62	35.00	Unknown	1	>20			Androgen deprivation therapy, Chemotherapy	Progression	245
20	63	3.00	Unknown					Radical prostatectomy and radiotherapy	Relapse	265
21	65	3.55	8		5	4		Radical prostatectomy, lymphadenectomy	Relapse	224
22	64	0.50	8		1			Radical prostatectomy	Relapse	232
23	74	0.14	7					Radical prostatectomy	Relapse	247
24	84	2.50	Unknown					Radical prostatectomy, androgen deprivation therapy	Progression	220
25	78	45.0	Unknown		9			Radical prostatectomy	Progression	144

Semi-quantitative evaluation was based on volumes of interest (VOIs) and on subsequent calculations of SUV values. VOIs were drawn with an isocontour mode (pseudo-snake) and were placed over sites suspected of PC involvement as well as over organs with physiologic tracer uptake such as the parotid glands, liver, spleen, kidneys, urinary bladder, and colon. Moreover, SUV calculations were performed for blood pool (common iliac artery), normal osseous tissue (iliac bone), and gluteal muscles (http://www.pmod.com/files/download/v31/doc/pbas/4729.htm).

Quantitative evaluation of the dynamic PET/CT data was based on irregular VOIs, drawn also with an isocontour mode (pseudo-snake), placed over foci indicative of PC involvement and was performed using a

dedicated software package [18, 19]. Time-activity curves (TACs) were created using VOIs. A detailed quantitative evaluation of tracer kinetics was performed based on a two-tissue compartment model [20, 21]. The accurate measurement of the input function requires arterial blood sampling. However, it can be retrieved relatively simplified and non-invasively from the image data with good accuracy according to methods already reported in literature [22]. For the input function, the mean value of the VOI data from the common iliac artery was used. A vessel VOI consisted of at least seven ROIs in sequential PET/CT images. The recovery coefficient was 0.85 for a diameter of 8 mm. Partial volume correction was performed for small vessels (diameter less than 8 mm) based on phantom measurements of the recovery function. The two-tissue compartment model describes tracer kinetics in the studied area and involves the plasma compartment (c_{plasma}), the free (unbound) component in interstitial and/or intracellular space (c_1), and the PSMA-specific component of the radiotracer (s_2). The constants K_1, k_2, k_3, and k_4 were calculated taking into account the vascular fraction in a VOI as an additional variable. In this model, K_1 and k_2 reflect the forward and reverse transport of the radiotracer between plasma and the "reversible" interstitial/intracellular compartment; k_3 is associated with tracer binding to the zinc active site of PSMA and its internalization via clathrin-mediated endocytosis, and k_4 represents dissociation of the tracer from the zinc active site of PSMA and externalization (Fig. 1) [5, 17, 23]. The unit for the rate constants K_1, k_2, k_3, and k_4 is 1/min. The model parameters were accepted when K_1, k_2, k_3, and k_4 were less than 1. The two-tissue compartment model we applied is a modification of the one proposed by Sokoloff et al., which did not take into account the parameters k_4 as well as blood volume (V_B), which is associated with the volume of blood exchanging with tissue [20]. This lack of k_4 and V_B, however, leads to different values of the parameters K_1 and k_3, since K_1 assessment is dependent on V_B, and k_3 assessment on k_4. Following compartmental analysis, we calculated the global influx (K_i) from the compartment data using the formula: $K_i = (K_1 \times k_3)/(k_2 + k_3)$. Kinetic analysis was performed over ^{18}F-PSMA-1007 avid foci indicative of malignant involvement, as well as over the urinary bladder, colon, reference bone (os ilium) and gluteal muscles.

Besides the compartmental analysis, fractal analysis, a non-compartment model, was used in order to calculate the parameter of heterogeneity and complexity, expressed by a non-integer value, so-called fractal dimension (FD). FD is calculated for the time-activity data in each individual voxel of a VOI. The values of the FD vary from 0 to 2 showing the deterministic or chaotic distribution of the tracer-associated activity with higher values being related to a more heterogeneous distribution of ^{18}F-PSMA-1007 [24].

Data were statistically evaluated using the SPSS v.20.0 (IBM Corp., Armonk, NY, USA) software. The statistical evaluation was performed using descriptive statistics, Wilcoxon rank-sum test, and Spearman's rank correlation analysis. The results were considered significant for p less than 0.05 ($p < 0.05$).

Results

Whole-body PET/CT studies

Patient-based evaluation

There were no reported adverse events associated with the application of ^{18}F-PSMA-1007. Of the 25 studied patients, 15 (60.0%) had at least one ^{18}F-PSMA-1007 positive PC lesion, while 10/25 patients (40.0%) were ^{18}F-PSMA-1007 negative. The median PSA value in the ^{18}F-PSMA-1007 positive group was 3.6 ng/mL (mean value = 23.5 ng/mL; range = 0.2–237.3 ng/mL; standard deviation = 14.8 ng/mL) and in the ^{18}F-PSMA-1007 negative group 0.7 ng/mL (mean value = 1.0 ng/mL; range = 0.1–3.0 ng/mL; standard deviation = 1.3 ng/mL). The differences between the two groups, in terms of PSA levels, were statistically significant.

Eight of the 17 patients with PC biochemical recurrence were ^{18}F-PSMA-1007 positive, while nine of them were ^{18}F-PSMA-1007 negative. Respectively, 7/8 patients with biochemical progression of PC were ^{18}F-PSMA-1007 positive and one patient was ^{18}F-PSMA-1007 negative (Figs. 2 and 3).

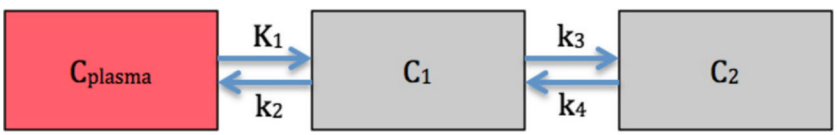

Fig. 1 Schematic representation of the two-tissue compartment model applied for ^{18}F-PSMA-1007. K_1, k_2, k_3, and k_4 are rate constants (1/min) and describe the directional exchanges between the three compartments (c_{plasma} represents the vascular compartment, c_1 represents the free-unbound component in the interstitial and/or intracellular space, c_2 represents the PSMA specific component of the radiotracer). K_1 and k_2 reflect the forward and reverse transport of the radiotracer between plasma and the "reversible" interstitial/intracellular compartment; k_3 is associated with tracer binding to the zinc active site of PSMA and its internalization via clathrin-mediated endocytosis, and k_4 represents dissociation of the tracer from the zinc active site of PSMA and externalization

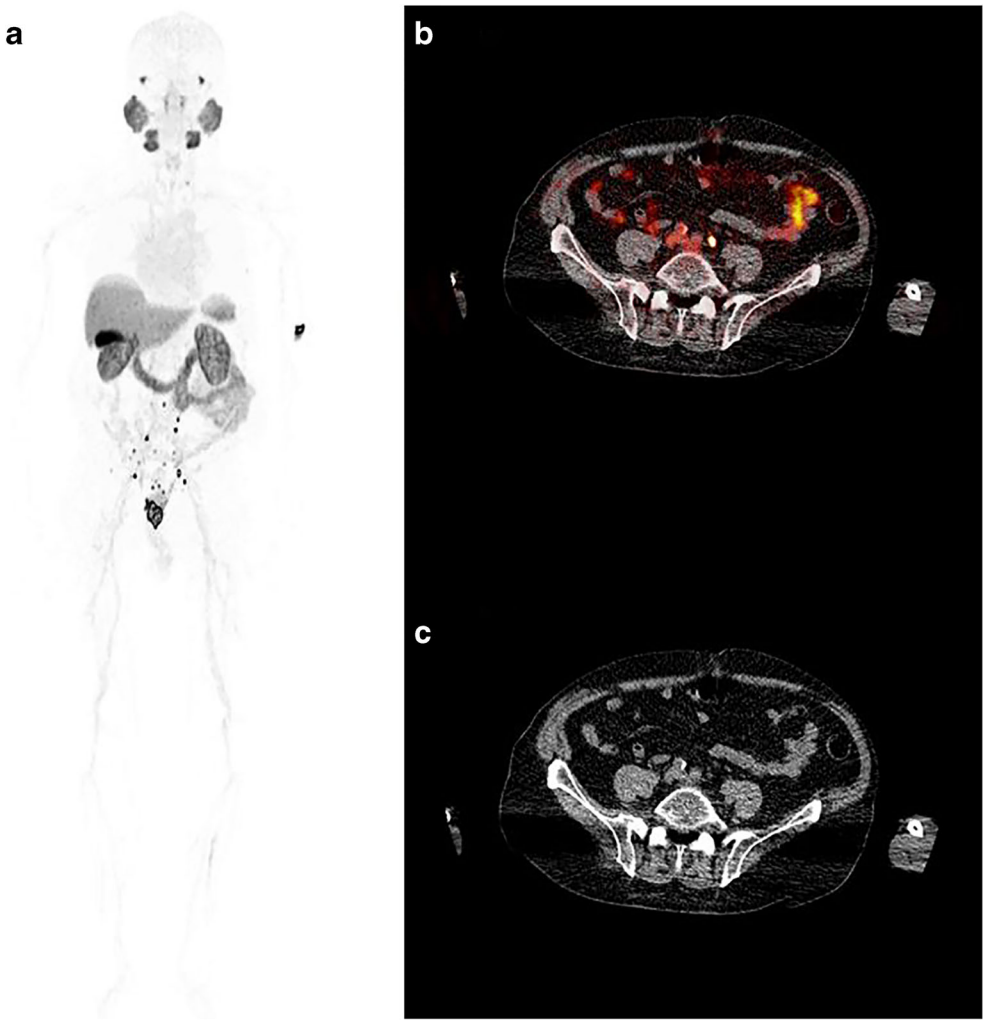

Fig. 2 A 79-year-old patient was referred to our department due to biochemical progression of PC and PSA elevation at 7.28 ng/mL. The patient was treated with radical prostatectomy and androgen deprivation therapy. ^{18}F-PSMA-1007 PET whole-body maximum intensity projection (MIP) (**a**) demonstrates multiple foci of increased tracer uptake in the abdomen and pelvis, corresponding to several lymph node metastases and a local relapse. Transaxial, fused ^{18}F-PSMA-1007 PET/CT at the pelvic level (**b**) shows a focal site of increased tracer uptake, corresponding to an iliac lymph node. Transaxial low-dose non-enhanced CT at the same level (**c**) shows no pathologic enlargement, at the anatomical site of the tracer accumulating iliac lymph node. The $SUV_{average}$ of the local relapse was 21.1 (SUV_{max} = 37.3) and of the lymph node metastases ranged from 10.1 to 21.8 (SUV_{max} range = 18.2–42.1). The respective SUV values for normal organs were the following: blood pool $SUV_{average}$ = 3.7 (SUV_{max} = 5.2), parotid gland $SUV_{average}$ = 16.2 (SUV_{max} = 27.2), liver $SUV_{average}$ = 8.9 (SUV_{max} = 17.4), spleen $SUV_{average}$ = 8.3 (SUV_{max} = 18.5), kidneys $SUV_{average}$ = 13.8 (SUV_{max} = 32.6), urinary bladder $SUV_{average}$ = 6.5 (SUV_{max} = 8.8), colon $SUV_{average}$ = 3.9 (SUV_{max} = 8.7), and gluteal muscles $SUV_{average}$ = 0.8 (SUV_{max} = 1.4)

Lesion-based evaluation

Visual evaluation Five patients with biochemical PC progression demonstrated disseminated metastatic disease: three patients had disseminated lymph node metastatic disease, one patient had disseminated lymph node and bone metastatic disease, while one patient had disseminated lymph node, osseous, and liver metastases; in these patients, the exact calculation of metastatic lesions was practically impossible. Regarding PC lesions in the remaining patients, six of them corresponded to local PC recurrence, 24 to lymph node metastases, nine to bone metastases, and one to lung metastasis (Table 1).

Semi-quantitative evaluation Semi-quantitatively evaluations were performed in 89 PC lesions demonstrated in whole-body, static PET/CT starting approximately at 70 min p.i. These lesions corresponded to 5 local PC recurrences, 52 lymph node metastases, 31 bone metastases, and 1 liver metastasis and revealed a mean $SUV_{average}$ of 25.1 (median = 15.4; range = 3.5–119.2) and a mean SUV_{max} of 41.5 (median = 25.7; range = 3.8–213.2). In particular, mean $SUV_{average}$ of local PC relapses was 22.2 (SUV_{max} = 42.0), of lymph node metastases 30.9 (SUV_{max} = 51.3), and of bone metastases 16.3 (SUV_{max} = 25.1). The SUV values of lymph node metastases were higher than those of bone metastases. No

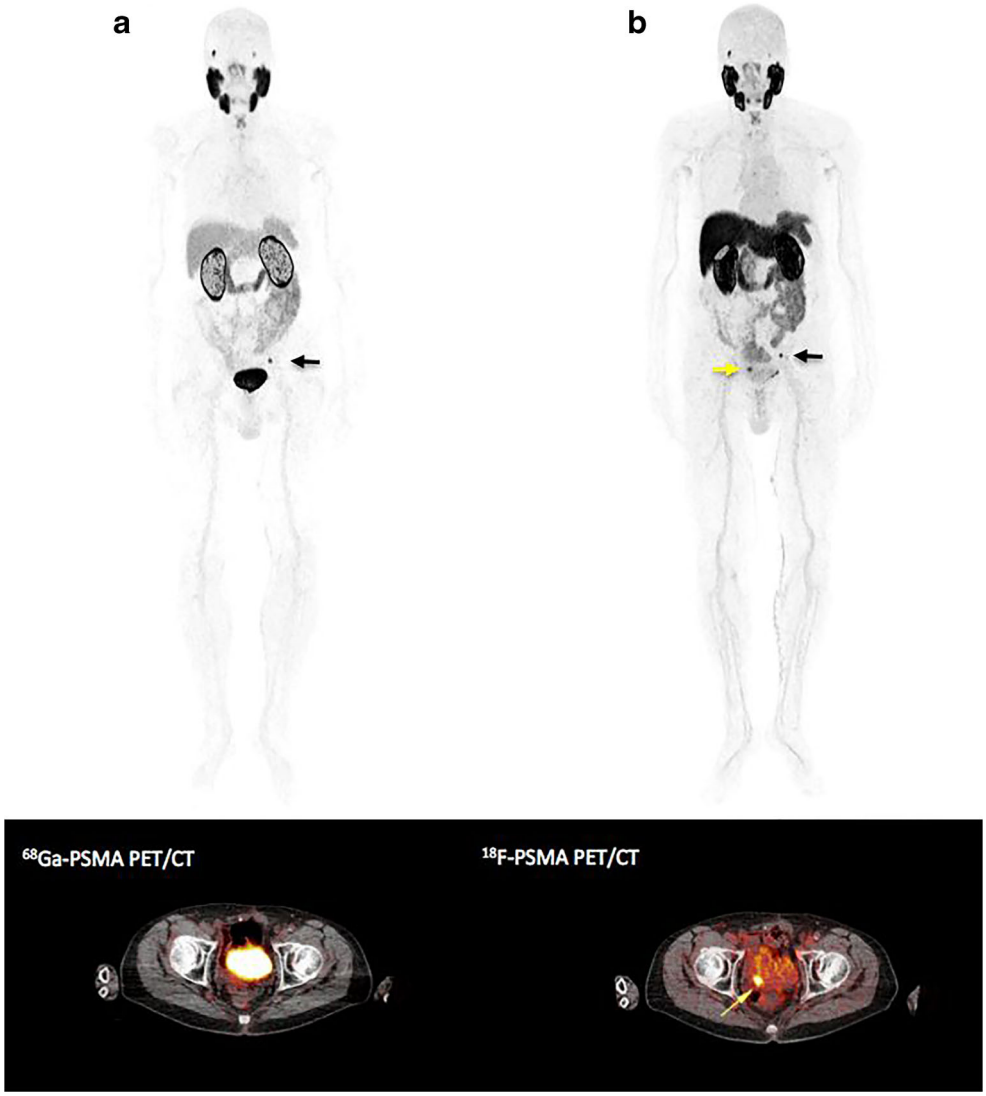

Fig. 3 A 71-year-old PC patient, who had undergone radical prostatectomy 1 year ago (Gleason score 10), was referred to our department due to a rise of PSA at 0.18 ng/mL. Whole-body maximum intensity projection (MIP) as well as transaxial ^{68}Ga-PSMA-11 PET/CT (**a**) demonstrate a left iliac lymph node metastasis (black arrow). ^{18}F-PSMA-1007 PET/CT performed 24 h later (**b**) revealed apart from the iliac lymph node metastasis, a focal site of increased tracer uptake, corresponding to local PC recurrence (yellow arrow) not seen on low-dose CT or ^{68}Ga-PSMA-11 PET/CT due to intense radiotracer accumulation in the urinary bladder. The patient had also one bone metastasis not clearly depicted on MIP

significant differences in SUV values were observed between PC lesions in patients with relapse or progression.

Apart from the PC lesions, SUV values were also calculated in normal tissues, in which PSMA ligands show a normally high distribution (parotid glands, liver, spleen, kidneys, urinary bladder, and colon) as well as in the gluteal muscles. The results of semi-quantitative analysis derived from static, whole body imaging are presented in Table 2. In general, SUV was higher in PC lesions than all other evaluated tissues, with these differences being also statistically significant ($p < 0.05$) when compared to the urinary bladder and the gluteus muscles.

Dynamic PET/CT studies of the lower abdomen and pelvis

No further lesions were detected in early images in comparison to static PET/CT in the anatomic area of the lower abdomen and pelvis. Forty-five (45) ^{18}F-PSMA-1007 positive lesions were quantitatively evaluated by means of dPET/CT: four locally recurrent PC lesions, 23 lymph node metastases, and 18 osseous metastases. Regarding the different PC recurrence sites, Wilcoxon rank-sum test revealed no significant differences regarding two-tissue compartment model-derived parameters. However, FD was significantly higher in lymph node metastases than osseous metastases ($p < 0.05$). No differences were observed between PC lesions in patients with relapse or progression. Median k_3 was 35-fold higher than k_4 in PC lesions ($p < 0.0001$). Table 3 demonstrates the values of the ^{18}F-PSMA-1007 kinetic parameters acquired from the PC lesions (local relapses, lymph node metastases, bone metastases) as well as from the urinary bladder, colon, reference bone, and gluteal muscles. Similar to semi-quantitative evaluations, PC lesions showed higher values for kinetic parameters and FD than the rest studied normal organs. These differences were also statistically significant when PC lesions were compared with the urinary bladder (FD), the colon (K_1, influx,

Table 2 Descriptive statistics of ^{18}F-PSMA-1007 SUV values derived from static, whole-body PET/CT starting approximately 70 min p.i. The mean (median) SUV values are derived from the 89 semi-quantitatively evaluated PC lesions as well as the physiologic parotid glands, liver, spleen, kidneys, urinary bladder, colon, and gluteal muscles

	$SUV_{average}$	SUV_{max}
PC lesions (total)	25.1 (15.4)	41.5 (25.7)
PC local recurrences	22.2 (9.4)	42.0 (14.6)
Lymph node metastases	30.9 (20.4)	51.3 (36.8)
Bone metastases	16.3 (10.7)	25.1 (19.4)
Kidney	16.3 (15.1)	32.1 (32.8)
Urinary bladder	4.4 (4.0)	6.9 (6.9)
Gluteus	0.7 (0.7)	1.2 (1.1)
Colon	5.4 (4.0)	9.3 (7.9)
Spleen	9.7 (8.6)	17.1 (17.8)
Liver	10.1 (9.8)	20.3 (17.9)
Parotid gland	18.1 (18.1)	29.5 (30.2)
Blood pool*	2.6 (3.0)	3.8 (3.6)

*Measured at 60 min p.i

FD), reference bone (k_3, influx, FD), and the gluteus muscles (K_1, FD).

The application of dPET/CT scanning led also to the extraction of time-activity curves (TACs), which show the activity concentration of ^{18}F-PSMA-1007 in the selected VOIs during the 60 min of dPET/CT acquisition (24 time points according to the defined frames). In general, almost all PC-lesion-derived curves showed that ^{18}F-PSMA-1007 concentration considerably increases in the respective VOIs over time. On the other hand, neither the urinary bladder nor the colon TACs showed a marked increasing accumulation of the tracer, which was definitely less than in the PC lesions. Tracer accumulation in normal bone and the reference gluteal muscles was negligible. Figure 4 demonstrates the resulting TACs based on the mean values and the standard deviation of all evaluated data derived from local relapses, lymph node metastases, osseous metastases, colon, urinary bladder, blood pool (drawn over the common iliac artery), normal bone (drawn over the iliac bone), as well as the gluteus musculature.

Spearman's rank correlation analysis was performed between ^{18}F-PSMA-1007 quantitative parameters. The strongest correlations ($p < 0.05$) were found between FD and $SUV_{average}$ ($r = 0.93$), FD and influx ($r = 0.85$), FD and SUV_{max} ($r = 0.83$), as well as between influx and $SUV_{average}$ ($r = 0.82$), and influx and SUV_{max} ($r = 0.75$).

Discussion

Localization of biochemical recurrence of PC has clinical impacts especially at low PSA levels, since early salvage radiotherapy and surgery of local disease provides a possibility of cure [25]. In the current decade, ^{68}Ga-PSMA-11 PET/CT has emerged as a promising modality in PC recurrence diagnostics, demonstrating unprecedented detection rates when compared with conventional imaging techniques even in patients with low PSA levels [2, 3, 7, 26, 27]. Although the main indication of ^{68}Ga-PSMA-11 PET/CT lies in the assessment of PC in the biochemical relapse setting, the modality is increasingly gaining importance also in the initial staging of the intermediate and high-risk disease as well as in the restaging of metastatic disease [28]. It is estimated that ^{68}Ga-PSMA-11 PET/CT leads to a change in therapeutic management of up to 54% of PC patients [29].

Most recently, the newly introduced ^{18}F-PSMA-1007 ligand has shown high detection rates in PC patients after radical prostatectomy, comparable to those of ^{68}Ga-PSMA-11 and, moreover, with favorable characteristics regarding both imaging and logistics [15]. In an attempt to widen the existing knowledge on ^{18}F-PSMA-1007 PET/CT in PC diagnostics, we herein evaluated the detection rates and the kinetics of the tracer in a cohort of 25 PC patients with either biochemical recurrence after therapy with curative intent or biochemical progression of known metastatic disease, by means of multiparametric PET/CT consisting of a combination of a dynamic and whole-body PET/CT protocol.

Patient-based analysis demonstrated that 60% of patients were ^{18}F-PSMA-1007 positive, with higher detection rates in patients with higher PSA. Notably, 28% ($n = 7$ patients) of the herein studied cohort had PSA values ≤ 0.5 ng/mL; in this subgroup, four patients were ^{18}F-PSMA-1007 negative, confirming the limitations of PSMA-radioligand imaging in patients with very low PSA values. Moreover, the here presented cohort is relatively heterogeneous, consisting of patients with first biochemical recurrence after radical prostatectomy ($n = 17$) as well as patients who had relapsed more than once and showed biochemical progression under systemic therapy ($n = 8$).

As expected, the radiotracer ^{18}F-PSMA-1007 showed a similar biodistribution pattern with the widely used tracer ^{68}Ga-PSMA-11 both in PC- and normally expressing PSMA-tissues (parotid glands, liver, spleen, kidneys). Nevertheless, they are not identical. The main differences between the two tracers lie, firstly, in the much lower excretion of ^{18}F-PSMA-1007 into the urinary bladder, which is a known drawback of ^{68}Ga-PSMA-11 potentially hampering its diagnostic efficacy in local recurrence and locoregional disease detection (Fig. 3). Importantly, in the present study, we could show a statistically significant higher ^{18}F-PSMA-1007 uptake (SUV) in PC lesions than in the urinary bladder. Secondly, due to its slightly higher lipophilic characteristics, ^{18}F-PSMA-1007 is cleared mainly via the hepatobiliary excretion route resulting in higher gallbladder and intestinal accumulation than in case of ^{68}Ga-PSMA-11. Anyhow, the tracer uptake

Table 3 Descriptive statistics of ^{18}F-PSMA-1007 kinetic parameters. The mean (median) kinetic parameters are derived from 45 pelvic PC lesions as well as the urinary bladder, colon, reference bone (os ilium), and gluteal muscles, after application of two-tissue compartment modeling in the dPET/CT data from the pelvis

	K_1 (1/min)	k_3 (1/min)	Influx-K_i (1/min)	FD
PC lesions (total)	0.11 (0.08)	0.17 (0.09)	0.05 (0.02)	1.29 (1.24)
PC local relapses	0.12 (0.12)	0.14 (0.14)	0.05 (0.02)	1.24 (1.24)
Lymph node metastases	0.18 (0.12)	0.26 (0.14)	0.09 (0.05)	1.31 (1.34)
Bone metastases	0.09 (0.08)	0.15 (0.08)	0.04 (0.02)	1.26 (1.24)
Urinary bladder	0.05 (0.04)	0.14 (0.13)	0.01 (0.02)	1.13 (1.14)
Colon	0.09 (0.06)	0.11 (0.06)	0.01 (0.01)	1.15 (1.16)
Reference bone	0.07 (0.07)	0.07 (0.03)	0.004 (0.004)	0.96 (0.99)
Gluteus	0.01 (0.01)	0.10 (0.11)	0.01 (0.003)	0.78 (0.77)

and the influx were higher in PC-lesions than in colon tissue. Another interesting result of semi-quantitative analysis was the higher tracer uptake of lymph node metastases in comparison to bone metastases, which may reflect a difference in the tumor biology of these types of metastases regarding PSMA expression.

The dynamic, early PET/CT acquisition (two bed positions) over the pelvis and the lower abdomen did not reveal more lesions in comparison to static PET/CT. This finding is in contrary with the experience in ^{68}Ga-PSMA-11 PET imaging, in which early PET imaging leads to increased detection rate of PC local recurrence due to lower tracer accumulation in the urinary bladder [30–32]. However, there exists yet no consensus on the optimal time point of imaging with ^{18}F-based PSMA radioligands. With the increasing routine clinical use of these tracers, the question of when to best perform ^{18}F-PSMA-1007 PET/CT is non-trivial. Thus, we expect that our finding of no further lesions detected with early PET imaging to be of significance, given the fact that performance of early dynamic imaging is time-consuming and quite demanding.

However, the subsequent application of two-tissue compartment modeling in the ^{18}F-PSMA-1007 dynamic PET/CT data led to the extraction of certain parameters, which describe tracer kinetics in detail. The biological distribution of PSMA ligands and their eventual internalization in the PC cell involve a sequence of steps. A goal of a kinetic model is to characterize such processes in a relatively simple manner. In this sense, the two-tissue compartment model we applied is an approximation (simplification) of the underlying biological system, involving the plasma compartment, a "reversible" interstitial/intracellular compartment, and an "irreversible," PSMA-specific compartment. A similar approach was applied in previous studies of our group using the tracer ^{68}Ga-PSMA-11 in patients with newly diagnosed PC [5] as well as PC biochemical recurrence [17, 23]. In this context, kinetic analysis revealed that PC lesions showed higher values than the rest studied normal organs for the parameters K_1, reflecting the transport of ^{18}F-PSMA-1007 between plasma and the interstitial/intracellular compartment, k_3, representing tracer binding to the zinc active site of PSMA, and internalization via clathrin-mediated endocytosis, and tracer influx. Moreover, the median k_3 in PC lesions was 35-fold higher than parameter k_4, which represents tracer dissociation from the "receptor" and externalization, practically reflecting a trapping of the radioligand in the PC cell. Finally, the TACs from PC recurrence lesions showed an increasing tracer accumulation during the 60 min of dynamic PET acquisition, higher than the one observed in the reference normal tissues.

Taken together, the here presented results provide insight in the pharmacokinetics of the radiofluorinated PSMA ligand, reflecting its high binding and internalization as well as its steadily increasing accumulation in the PC lesions, findings which are in line with the ones published for ^{68}Ga-PSMA-11 dPET/CT. This observation could find its clinical translation in the rapidly evolving field of radiothera(g)nostics and, in particular, in the potential employment of ^{18}F-PSMA-1007 PET for the identification of patients with lesions carrying the characteristics of high tracer-associated binding and internalization in tumor tissue. Such patients would be suitable candidates for PSMA-targeted therapies with ^{177}Lu- and ^{225}Ac-labeled versions of PSMA ligands such as PSMA-617 [33–36].

In addition to two-tissue compartment modeling for evaluation of ^{18}F-PSMA-1007 kinetics, we adopted a non-compartmental method to extrapolate fractal indices that represent tissue heterogeneity. Unlike Euclidean geometry, fractal geometry can describe with higher approximation complex natural structures and biological dynamic processes [37, 38], which is particularly important in tumor biology characterized by the complexity of cellular systems [39]. In recent years, investigators have used fractal analysis for evaluation of tracer uptake in oncological imaging by means of PET with promising results [40–44].

In our analysis, FD is calculated for the time-activity data in each individual voxel of a VOI. This model measures the complexity of a dimensional structure by calculating its FD based on the box counting method [45]. This fractal approach gives evidence of the more chaotic or deterministic nature of PSMA expression and uptake, and can be used to estimate the heterogeneity of PET data, expressed by the parameter FD. The basic concept in the present analysis is that an increased FD is indicative of a more chaotic tracer distribution,

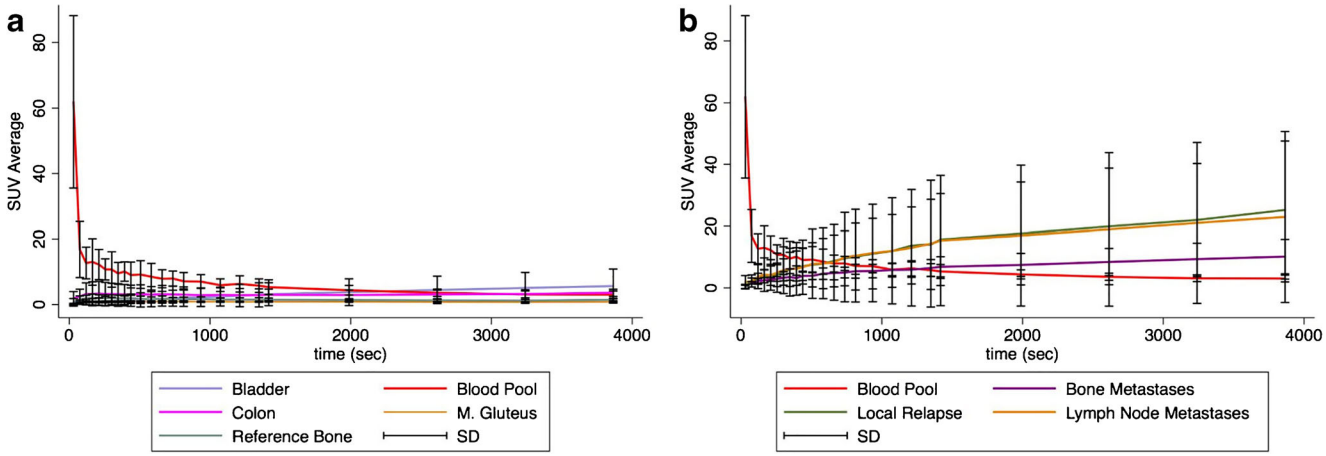

Fig. 4 Time-activity curves (TACs) derived from dynamic PET/CT studies of the pelvis using a 24-frame protocol (*y*-axis, $SUV_{average}$; *x*-axis, time in sec). The TACs represent the mean values and their standard deviation (SD) of all evaluated VOIs corresponding to physiologic tissues, including the urinary bladder, colon, normal/reference bone (drawn over the iliac bone), blood pool (drawn over the common iliac artery), and the gluteus musculature (**a**), as well as all evaluated PC-associated lesions, including local relapses, lymph node metastases, and osseous metastases (**b**). The curves derived from the normal tissues demonstrate a stable, low tracer concentration with the exception of the urinary bladder, which exhibits a small increase during dynamic PET/CT (**a**). On the other hand, the TACs derived from PC-associated lesions' VOIs show an increasing ^{18}F-PSMA-1007 accumulation within the 60 min of dynamic PET acquisition

reflecting a more heterogeneous distribution of the PSMA radioligand, meaning also an apparently more heterogeneous distribution of upregulated PSMA in tumor tissue. We could show that the degree of this heterogeneity was higher in PC lesions than in the other studied organs (urinary bladder, colon, and gluteus muscles). Furthermore, a strong correlation between ^{18}F-PSMA-1007 heterogeneity and the amount of tracer uptake (SUV) and influx (K_i) as well as a moderate correlation with the binding rate of the tracer on the surface protein PSMA (K_1) in tumor lesions was demonstrated. These results are in accordance with previous data published from our group regarding the application of fractal analysis in ^{68}Ga-PSMA-11 dPET/CT studies in patients with primary and recurrent PC [5, 17, 23].

Although the potential of fractal mathematics in oncological research and practice remains relatively unknown to most clinicians, the so far gathered experience from our as well as other groups indicates that tumor heterogeneity—determined after applying fractal principles on PET images—can serve as a novel imaging biomarker of tumor biodiversity with, potential prognostic survival implications [43, 46–48]. In addition, the determination of FD may have an impact on the selection of patients for PSMA radioligand therapy.

Our analysis has some limitations. Firstly, the studied cohort is relatively small and mixed including patients with biochemical recurrence and patients with a PSA progression under therapy. We acknowledge that results of quantitative analysis could be influenced in the group examined with ongoing androgen deprivation therapy. However, almost all PC lesions studied in patients—with or without treatment—showed a similar pattern regarding ^{18}F-PSMA-1007 pharmacokinetics. A second limitation is the lack of histological confirmation of the ^{18}F-PSMA-1007 avid focal lesions in cases of local relapse after curative treatment, since these lesions are quite small to biopsy. Nevertheless, results from a recent similar study have shown a high correlation between imaging and histopathologic findings [11]. Moreover, despite the lack of sufficient data to evaluate the significance of SUV in terms of potential differentiation between malignant and benign findings in ^{18}F-PSMA-1007 PET, the gathered experience with ^{68}Ga-PSMA-11 PET suggests that higher SUV values most probably reflect PC-associated lesions. This is based on the knowledge that higher SUV values are a result of high PSMA receptor expression, which is in turn highly correlated with malignancy [49]. Finally, dynamic sequences were performed only in the lower abdomen and the pelvis, and not over the whole body, depriving us of kinetic data from distant lesions. The advent of new PET/CT scanners, using a continuous movement and allowing dynamic studies over several bed positions, will facilitate the use of dynamic PET protocols and reduce the acquisition time.

Conclusion

We performed ^{18}F-PSMA-1007 PET/CT in a group of 25 PC patients with biochemical relapse or progression, including also patients with very low PSA values. ^{18}F-PSMA-1007 PET/CT localized PC lesions in 60% of the studied patients. Higher PSA values were associated with a higher detection rate. Although no further ^{18}F-PSMA-1007 positive lesions were detected by early, dynamic PET/CT, we could show that

tracer accumulation during the dynamic PET acquisition was higher in PC lesions than physiological tissues and, in particular, the urinary bladder and the colon, which represent the organs that can potentially hamper the diagnostic efficacy of the PSMA radioligands in the lower abdomen and pelvis. Moreover, pharmacokinetic analysis revealed an increasing tracer uptake, an apparently high binding and internalization as well as increased tracer heterogeneity of the radiofluorinated PSMA ligand in the PC lesions, providing further insight into the underlying biological processes and defining the pharmacokinetics of ^{18}F-PSMA-1007.

Compliance with ethical standards

Conflict of interest The clinical development of ^{18}F-PSMA-1007 is partly funded by a grant of the Federal Ministry of Education and Research (BMBF), project ProstaPET (2U2WTZKOREA-021; no. 01DR17031A).

Uwe Haberkorn and Klaus Kopka are inventors within a patent application for PSMA-1007. Other potential declarations of interest relevant to this article do not exist.

Ethical approval All procedures performed in studies involving human participants were in accordance with the ethical standards of the institutional and/or national research committee and with the 1964 Helsinki declaration and its later amendments or comparable ethical standards.

Informed consent Informed consent was obtained from all individual participants included in the study.

References

1. Afshar-Oromieh A, Zechmann CM, Malcher A, et al. Comparison of PET imaging with a (68)Ga-labelled PSMA ligand and (18)F-choline-based PET/CT for the diagnosis of recurrent prostate cancer. Eur J Nucl Med Mol Imaging. 2014;41:11–20.
2. Afshar-Oromieh A, Avtzi E, Giesel FL, et al. The diagnostic value of PET/CT imaging with the (68)Ga-labelled PSMA ligand HBED-CC in the diagnosis of recurrent prostate cancer. Eur J Nucl Med Mol Imaging. 2015;42:197–209.
3. Eiber M, Maurer T, Souvatzoglou M, et al. Evaluation of hybrid 68Ga-PSMA-ligand PET/CT in 248 patients with biochemical recurrence after radical prostatectomy. J Nucl Med. 2015;56:668–74.
4. Maurer T, Gschwend JE, Rauscher J, et al. Diagnostic efficacy of 68Gallium-PSMA-PET compared to conventional imaging in lymph node staging of 130 consecutive patients with intermediate to high risk prostate cancer. J Urol. 2016;195(5):1436–43.
5. Sachpekidis C, Kopka K, Eder M, et al. 68Ga-PSMA-11 Dynamic PET/CT imaging in primary prostate cancer. Clin Nucl Med. 2016;41(11):e473–9.
6. Uprimny C, Kroiss AS, Decristoforo C, et al. 68Ga-PSMA-11 PET/CT in primary staging of prostate cancer: PSA and Gleason score predict the intensity of tracer accumulation in the primary tumour. Eur J Nucl Med Mol Imaging. 2017;44(6):941–9.
7. Afshar-Oromieh A, Holland-Letz T, Giesel FL, et al. Diagnostic performance of 68Ga-PSMA-11 (HBED-CC) PET/CT in patients with recurrent prostate cancer: evaluation in 1007 patients. Eur J Nucl Med Mol Imaging. 2017;44(8):1258–68.
8. Pandey MK, Byrne JF, Jiang H, Packard AB, DeGrado TR. Cyclotron production of (68)Ga via the (68)Zn(p,n)(68)Ga reaction in aqueous solution. Am J Nucl Med Mol Imaging. 2014;4(4):303–10.
9. Freitag MT, Radtke JP, Afshar-Oromieh A, et al. Local recurrence of prostate cancer after radical prostatectomy is at risk to be missed in 68Ga-PSMA-11-PET of PET/CT and PET/MRI: comparison with mpMRI integrated in simultaneous PET/MRI. Eur J Nucl Med Mol Imaging. 2017;44(5):776–87.
10. Giesel FL, Hadaschik B, Cardinale J, et al. F-18 labelled PSMA-1007: biodistribution, radiation dosimetry and histopathological validation of tumor lesions in prostate cancer patients. Eur J Nucl Med Mol Imaging. 2017;44:678–88.
11. Giesel F, Will L, Lawal I, et al. Intra-individual comparison of 18F-PSMA-1007 and 18F-DCFPyL PET/CT in the prospective evaluation of patients with newly diagnosed prostate carcinoma: a pilot study. J Nucl Med. 2018;59:1076–80.
12. Giesel FL, Will L, Kesch C, et al. Biochemical recurrence of prostate cancer: initial results with [18F]PSMA-1007 PET/CT. J Nucl Med. 2018;59(4):632–5.
13. Rahbar K, Afshar-Oromieh A, Seifert R, Wagner S, Schäfers M, Bögemann M, et al. Diagnostic performance of 18F-PSMA-1007 PET/CT in patients with biochemical recurrent prostate cancer. Eur J Nucl Med Mol Imaging. 2018;45(12):2055–61.
14. Rahbar K, Afshar-Oromieh A, Bögemann M, et al. 18F-PSMA-1007 PET/CT at 60 and 120 minutes in patients with prostate cancer: biodistribution, tumour detection and activity kinetics.
15. Giesel FL, Knorr K, Spohn F, et al. Detection efficacy of [18F]PSMA-1007 PET/CT in 251 Patients with biochemical recurrence after radical prostatectomy. J Nucl Med. 2019;60(3):362–8.
16. Cardinale J, Martin R, Remde Y, et al. Procedures for the GMP-compliant production and quality control of [18F]PSMA-1007: a next generation radiofluorinated tracer for the detection of prostate cancer. Pharmaceuticals (Basel). 2017;10(4):77.
17. Sachpekidis C, Eder M, Kopka K, et al. (68)Ga-PSMA-11 dynamic PET/CT imaging in biochemical relapse of prostate cancer. Eur J Nucl Med Mol Imaging. 2016;43(7):1288–99.
18. Burger C, Buck A. Requirements and implementations of a flexible kinetic modeling tool. J Nucl Med. 1997;38:1818–23.
19. Mikolajczyk K, Szabatin M, Rudnicki P, Grodzki M, Burger C. A Java environment for medical image data analysis: initial application for brain PET quantitation. Med Inf. 1998;23:207–14.
20. Sokoloff L, Smith CB. Basic principles underlying radioisotopic methods for assay of biochemical processes in vivo. In: Greitz T, Ingvar DH, Widén L, editors. The metabolism of the human brain studied with positron emission tomography. New York: Raven Press; 1983. p. 123–48.
21. Miyazawa H, Osmont A, Petit-Taboué MC, et al. Determination of 18F-fluoro-2-deoxy-D-glucose rate constants in the anesthetized baboon brain with dynamic positron tomography. J Neurosci Methods. 1993;50:263–72.
22. Ohtake T, Kosaka N, Watanabe T, et al. Noninvasive method to obtain input function for measuring tissue glucose utilization of thoracic and abdominal organs. J Nucl Med. 1991;32:1432–8.
23. Sachpekidis C, Bäumer P, Kopka K, et al. 68Ga-PSMA PET/CT in the evaluation of bone metastases in prostate cancer. Eur J Nucl Med Mol Imaging. 2018;45(6):904–12.
24. Dimitrakopoulou-Strauss A, Strauss LG, Burger C, Mikolajczyk K, Lehnert T, et al. On the fractal nature of positron emission tomography (PET) studies. World J Nucl Med. 2003;4:306–13.
25. Cornford P, Bellmunt J, Bolla M, et al. EAU-ESTRO-SIOG Guidelines on Prostate Cancer. Part II: treatment of relapsing, metastatic, and castration-resistant prostate cancer. Eur Urol. 2017;71:630–42.
26. Hoeks CMA, Barentsz JO, Hambrock T, et al. Prostate cancer: multiparametric MR imaging for detection, localization, and staging. Radiology. 2011;261:46–66.

27. Beer AJ, Eiber M, Souvatzoglou M, Schwaiger M, Krause BJ. Radionuclide and hybrid imaging of recurrent prostate cancer. Lancet Oncol. 2011;12:181–91.
28. Maurer T, Gschwend JE, Rauscher I, et al. Diagnostic efficacy of (68)Gallium-PSMA positron emission tomography compared to conventional imaging for lymph node staging of 130 consecutive patients with intermediate to high risp prostate Cancer. J Urol. 2016;195(5):1436–43.
29. Sheikhbahaei S, Afshar-Oromieh A, Eiber M, et al. Pearls and pitfalls in clinical interpretation of prostate-specific membrane antigen (PSMA)-targeted PET imaging. Eur J Nucl Med Mol Imaging. 2017;44(12):2117–36.
30. Uprimny C, Kroiss AS, Decristoforo C, et al. Early dynamic imaging in 68Ga- PSMA-11 PET/CT allows discrimination of urinary bladder activity and prostate cancer lesions. Eur J Nucl Med Mol Imaging. 2017;44(5):765–75.
31. Uprimny C, Kroiss AS, Fritz J, et al. Early PET imaging with [68]Ga-PSMA-11 increases the detection rate of local recurrence in prostate cancer patients with biochemical recurrence. Eur J Nucl Med Mol Imaging. 2017;44(10):1647–55.
32. Sachpekidis C, Pan L, Hadaschik BA, et al. 68Ga-PSMA-11 PET/CT in prostate cancer local recurrence: impact of early images and parametric analysis. Am J Nucl Med Mol Imaging. 2018;8(5):351–9.
33. Rahbar K, Ahmadzadehfar H, Kratochwil C, Haberkorn U, Schäfers M, et al. German multicenter study investigating 177Lu-PSMA-617 radioligand therapy in advanced prostate cancer patients. J Nucl Med. 2017;58:85–90.
34. Hofman MS, Violet J, Hicks RJ, et al. [177Lu]-PSMA-617 radionuclide treatment in patients with metastatic castration-resistant prostate cancer (LuPSMA trial): a single-centre, single-arm, phase 2 study. Lancet Oncol. 2018;19(6):825–33.
35. Kratochwil C, Bruchertseifer F, Giesel FL, Weis M, Verburg FA, et al. 225Ac-PSMA-617 for PSMA-targeted α-radiation therapy of metastatic castration-resistant prostate cancer. J Nucl Med. 2016;57:1941–4.
36. Sathekge M, Bruchertseifer F, Knoesen O, et al. 225Ac-PSMA-617 in chemotherapy-naive patients with advanced prostate cancer: a pilot study. Eur J Nucl Med Mol Imaging. 2018;46:129–38.
37. Mandelbrot B. How long is the coast of Britain? Statistical selfsimilarity and fractional dimension. Science. 1967;156:636–8.
38. Glenny RW, Robertson HT, Yamashiro S, Bassingthwaighte JB. Applications of fractal analysis to physiology. J Appl Physiol. 1991;70:2351–67.
39. Sedivy R. Fractal tumours: their real and virtual images. Wien Klin Wochenschr. 1996;108:547–51.
40. Di Ieva A, Grizzi F, Tschabitscher M, et al. (2010) correlation of microvascular fractal dimension with positron emission tomography [11C]-methionine uptake in glioblastoma multiforme: preliminary findings. Microvasc Res. 2010;80:267–73.
41. Miwa K, Inubushi M, Wagatsuma K, Nagao M, Murata T, Koyama M, et al. FDG uptake heterogeneity evaluated by fractal analysis improves the differential diagnosis of pulmonary nodules. Eur J Radiol. 2014;83:715–9.
42. Ben Bouallegue F, Tabaa YA, Kafrouni M, et al. Association between textural and morphological tumor indices on baseline PET-CT and early metabolic response on interim PET-CT in bulky malignant lymphomas. Med Phys. 2017;44:4608–19.
43. Tochigi T, Shuto K, Kono T, et al. Heterogeneity of glucose metabolism in esophageal cancer measured by fractal analysis of fluorodeoxyglucose positron emission tomography image: correlation between metabolic heterogeneity and survival. Dig Surg. 2017;34:186–91.
44. Lopci E, Grizzi F, Russo C, et al. Early and delayed evaluation of solid tumours with 64Cu-ATSM PET/CT: a pilot study on semi-quantitative and computer-aided fractal geometry analysis. Nucl Med Commun. 2017;38:340–6.
45. Peitgen HO, Juergens H, Saupe D. Length, area and dimension: measuring complexity and scaling properties. In: Peitgen HO, Juergens H, Saupe D, editors. Chaos and fractals. 1st ed. New York: Springer; 1992. p. 192–219.
46. Dimitrakopoulou-Strauss A, Strauss LG, Burger C, Rühl A, Irngartinger G, Stremmel W, et al. Prognostic aspects of 18F-FDG PET kinetics in patients with metastatic colorectal carcinoma receiving FOLFOX chemotherapy. J Nucl Med. 2004;45:1480–7.
47. Sachpekidis C, Hillengass J, Goldschmidt H, Wagner B, Haberkorn U, Kopka K, et al. Treatment response evaluation with 18F-FDG PET/CT and 18F-NaF PET/CT in multiple myeloma patients undergoing high-dose chemotherapy and autologous stem cell transplantation. Eur J Nucl Med Mol Imaging. 2017;44:50–62.
48. Castello A, Russo C, Grizzi F, Qehajaj D, Lopci E. Prognostic impact of intratumoral heterogeneity based on fractal geometry analysis in operated NSCLC patients. Mol Imaging Biol. 2018. https://doi.org/10.1007/s11307-018-1299-3.
49. Woythal N, Arsenic R, Kempkensteffen C, Miller K, Janssen JC, Huang K, et al. Immunohistochemical validation of PSMA expression measured by (68)Ga-PSMA PET/CT in primary prostate cancer. J Nucl Med. 2018;59(2):238–43.